Inference of Ice Cloud Properties From High Spectral Resolution Infrared Observations

Hung-Lung Huang, Ping Yang, Heli Wei, Bryan A. Baum, Yongxiang Hu, Paolo Antonelli, and Steven A. Ackerman

***Abstract*—The theoretical basis is explored for inferring the microphysical properties of ice clouds from high spectral resolution infrared (IR) observations. Extensive radiative transfer simulations are carried out to address relevant issues. The single-scattering properties of individual ice crystals are computed from state-of-the-art light scattering computational methods and are subsequently averaged for 30 *in situ* particle size distributions and for four additional analytical Gamma size distributions. The nonsphericity of ice crystals is shown to have a significant impact on the radiative signatures in the IR spectrum. Furthermore, the errors associated with the use of the Henyey–Greenstein phase function can be larger than 1 K in terms of brightness temperature for large particle effective sizes ($\sim$ 80 μm) at wavenumbers where the scattering of the IR radiation by ice crystals is not negligible. The simulations undertaken in this paper show that the slope of the IR brightness temperature spectrum between 790–960 cm^{-1} is sensitive to the effective particle size. Furthermore, a strong sensitivity of the IR brightness temperature to cloud optical thickness is noted within the 1050–1250-cm^{-1} region. Based on these spectral features, a technique is presented for the simultaneous retrieval of the visible optical thickness and effective particle size from high spectral resolution IR data for ice clouds. An error analysis shows that the uncertainties of the retrieved optical thickness and effective particle size have a small range of variation. The error for retrieving particle size in conjunction with an uncertainty of 5 K in cloud temperature, or a surface temperature uncertainty of 2.5 K, is less than 15%. The corresponding errors in the uncertainty of optical thickness are within 5% to 20%, depending on the value of cloud optical thickness. The applicability of the present retrieval technique is demonstrated using airborne high-resolution IR measurements obtained during two field campaigns.**

***Index Terms*—Ice Clouds, infrared spectrum, retrieval.**

I. Introduction

ICE CLOUDS play an important role in our climate system [1]–[4] yet their full impact on weather and climate change remains a puzzle. Substantial efforts have been focused on the remote sensing of ice clouds. Radiances observed by satellite-borne sensors at visible (Vis), near-infrared (NIR), and mid-infrared wavelengths are widely used to retrieve cloud properties [5]–[9]. Emitted infrared (IR) radiation, particularly in the atmospheric window region (i.e., 8–12 μm), contains a wealth of information on the properties of ice clouds. In the near future, our ability to observe these clouds will be substantially enhanced with the launch of new satellite instruments featured with high-spectral-resolution capability, such as the Geosynchronous Imaging Fourier Transform Spectrometer (GIFTS) [10], [11] and Cross-Track Infrared Sounder (CrIS) [12].

High-resolution spectral signatures in the atmospheric window region have been used previously to study cloud and aerosol properties. Ou *et al.* [13] presented an algorithm to infer ice cloud properties from Airborne Remote Earth Sensing system (ARES) data within two mid-IR atmospheric window (5.1–5.3- and 3.7-μm) bands. Various IR algorithms to infer ice cloud properties based on radiances within the 8–12 μm atmospheric window have been suggested (see [14]–[16]). A number of these studies, such as Chung *et al.* [14] and DeSlover *et al.* [17], approximated ice particles as spheres for the determination of scattering properties. However, Kahn *et al.* [18] found that radiative transfer simulations performed with nonspherical ice particle scattering models fit observed transmission spectra more accurately than the simulations based on the spherical approximation employed in light scattering computations. A similar conclusion was reached by Eldering *et al.* [19] who used high-resolution spectra of nongas-absorption transmission from Atmospheric Trace Molecule Spectroscopy Experiment (ATMOS) sun occultation data for ice cloud identification. Rathke and Fischer [20] presented an algorithm for inferring water cloud microphysical properties from high-resolution IR spectra, and investigated the sensitivity of the retrievals for clouds of moderate optical thickness.

The intent of the present study is to suggest an approach for simultaneously retrieving ice cloud microphysical properties from aircraft-based interferometer measurements in the 750–1250-cm^{-1} (i.e., 8–13.3 μm) spectral region. Our approach is complementary to those based on the Vis and NIR spectral signatures reported by Nakajima and King [5], King *et al.* [6] and Platnick *et al.* [7].

This paper proceeds as follows. Section II presents the methodology for deriving the single-scattering properties of ice crystals and the numerical model for IR radiative transfer. This section also discusses the effect of ice crystal nonsphericity and the Henyey–Greenstein (H–G) phase function representation of the phase function in the IR atmospheric window region.

Manuscript received August 28, 2003; revised November 3, 2003. This work was supported by the GIFTS-IOMI MURI Project. The work of P. Yang was supported also in part by the National Aeronautics and Space Administration (NASA) Radiation Sciences Program under Research Grants NAG-1–02002 and NAG5–11374, in part by the National Science Foundation under CAREER Award ATM-0239605, and in part by the NASA Cloud Aerosol Lidar and Infrared Pathfinder Observations (CALIPSO) Project.

H.-L. Huang, P. Antonelli, and S. A. Ackerman are with the Cooperative Institute for Meteorological Satellite Studies, University of Wisconsin, Madison, WI 53706 USA.

P. Yang and H. Wei are with the Department of Atmospheric Sciences, Texas A&M University, College Station, TX 77843 USA (e-mail: pyang@ariel.met.tamu.edu).

B. A. Baum and Y. Hu are with the NASA Langley Research Center, Hampton, VA USA 23681 and also with the Cooperative Institute for Meteorological Satellite Studies, University of Wisconsin, Madison, WI 53706 USA.

Digital Object Identifier 10.1109/TGRS.2003.822752

Section III presents the theoretical basis for inferring the microphysical and optical properties of ice clouds. Simulations are performed to understand the sensitivity of brightness temperatures to the optical thickness and particle effective size of ice clouds. An error analysis for our algorithm is presented in Section III where various factors that affect the retrieval accuracy are discussed. Shown in Section IV are two example cases for the simultaneous retrieval of the ice cloud effective particle size and optical thickness that were observed during the SUbsonic aircraft: Contrail and Cloud Effects Special Study (SUCCESS) in 1996 and the First International Satellite Cloud Climatology Project (ISCCP) Regional Experiment–Arctic Clouds Experiment (FIRE-ACE) in 1998. Finally, this study is summarized in Section V.

II. Single-Scattering Properties of Ice Clouds and Radiative Transfer Simulations

To infer cloud properties from satellite- or aircraft-borne IR interferometer observations, the radiance measurements are compared to theoretical simulations using a radiative transfer model (including a single-scattering module) that we describe in this section.

A. Single-Scattering Properties of Ice Clouds

Scattering by ice crystals in the IR spectral region is nonnegligible [21]. The single-scattering properties of ice crystals are essential to the simulation of the upwelling IR radiances. Although various *in situ* observations have demonstrated that ice clouds are almost exclusively composed of nonspherical ice crystals (e.g., [22] and [23]), studies involving IR radiance measurements often assume ice particles to be spherical. Simulation studies by Chung *et al.* [14] found that the assumption of a spherical geometry for ice crystals may be adequate for very small ice crystals at the IR wavelengths.

Heymsfield and Iaquinta [23] showed that in the upper portions of cirrus clouds, where the temperatures tend to be extremely cold and updraft velocities tend to be low, the ice particles are small. Although these small particles are nonspherical, they tend to have aspect ratios (i.e., the ratio of particle length to its width) close to unity. Yang *et al.* [24] suggested the shape of small ice crystals may be represented by the droxtal geometry. *In situ* measurements from the FIRE-II held in Coffeyville, KS in 1991, have shown that the middle to upper regions of midlatitude cirrus clouds are often composed of droxtals and pristine hexagonal crystals (see [23, Fig. 15]). This is an important observation since the upwelling radiance in the IR spectral region tends to be dominated by absorption and scattering from the middle to upper regions of the cloud.

In this paper, we use droxtals to represent small particles with sizes up to 32 μm in terms of the particle maximum dimension, and hexagonal columns to represent larger particles. A number of investigators assumed that ice crystals are hexagonal as a traditional way of defining nonspherical ice particle geometry. Yang *et al.* [25] reported the single-scattering properties of hexagonal ice crystals in the IR window region.

Scattering and absorption properties of droxtals and small hexagonal ice crystals are calculated using the finite-difference time-domain (FDTD) method [26]. Fig. 1 shows a comparison of the scattering phase functions at a wavenumber of 1250 cm^{-1} for spherical, droxtal, and hexagonal (with an aspect ratio of 1) ice crystal particles with the same maximum dimension of 10 μm. The phase function of the spherical particle was calculated from the Lorenz–Mie scattering computational code developed by Wiscombe [27]. As shown in Fig. 1, the scattering phase function is different for the three particle geometries in the forward and backward directions. The forward scattering by droxtals is smaller than that by either hexagonal or spherical crystals because the volume of the droxtal is the smallest for the same maximum dimension. The positions of scattering sub-maxima are different for the three types of crystals.

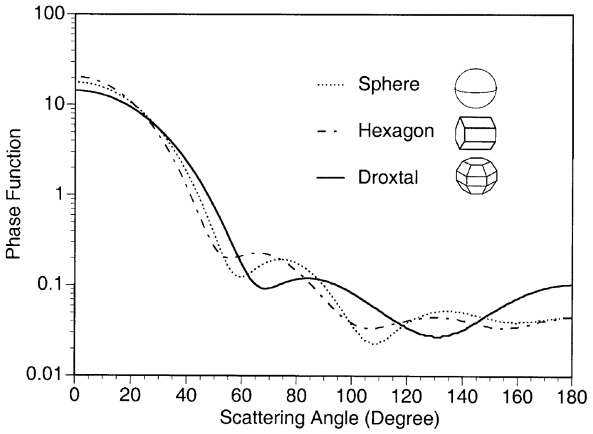

Fig. 1. Comparison of phase functions for droxtals, hexagonal columns, and spherical ice crystals with maximum dimension 10 μm at a wavenumber of 1250 cm^{-1} (wavelength 8.0 μm).

The extinction and absorption efficiencies for crystals ranging from 35–10 000 μm in size are derived on the basis of the composite approach originally developed by Fu *et al.* [28]. For small particles, the FDTD method is used to calculate the single-scattering properties. For larger particles, the weighted summation of approximate solutions may be used, such as those from the geometric optics method (GOM) or the equivalent-sphere approximation based on the Lorentz–Mie theory. The corresponding phase functions for larger particle sizes are derived from an improved geometric optics (IGOM) [29]. We notice that the difference between the phase function computed from IGOM and that from an asymptotic solution [30] are quite similar for the spectral region involved in this paper, if the size of the crystals is larger than approximately 40 μm. A recent study by Lee *et al.* [31] has confirmed the applicability of the IGOM for IR phase function computations in the case of circular cylinders, as validated by the T-matrix method [32].

The bulk ice cloud single-scattering properties are obtained by integrating the individual crystal scattering properties over 30 particle size distributions obtained during various campaigns for ice clouds from Fu [33] and Mitchell *et al.* [34]. Because no *in situ* measurements are available for clouds at extremely low temperatures (expected to contain primarily small ice particles), we assume very cold clouds composed of small particles to follow Gamma analytical distributions with effective sizes of 6, 8, 10, and 12 μm. Fu and Sun [35] found that the retrieval of effective size (D_e) is also sensitive to the ice particle size dis-

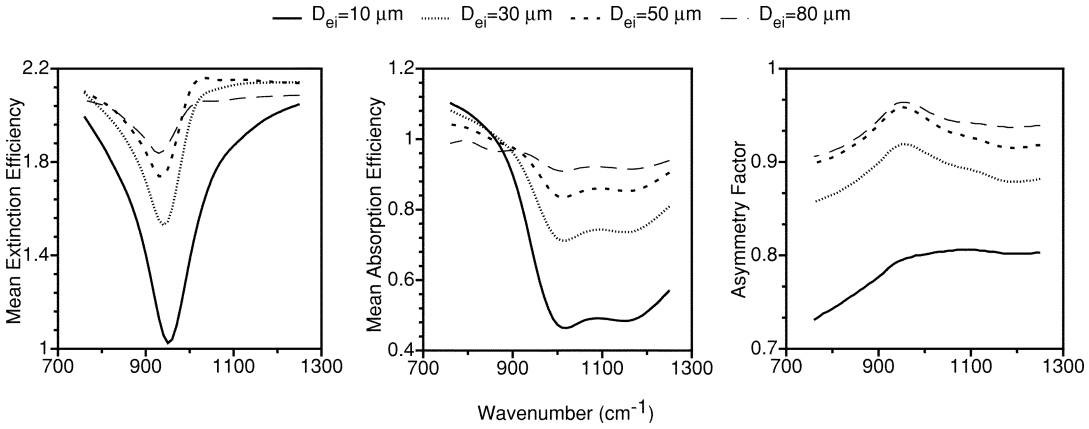

Fig. 2. Single-scattering properties of ice clouds for four effective particle sizes.

tribution assumed for ice crystals. The ice clouds at different geographic regions may have different size distributions due to differences in the thermodynamic and dynamic environments in which they form. Thus, a broad set of ice cloud particle size distributions are needed for the radiative transfer simulations involved in the retrieval process. The impact of the particle size distribution on the retrieval result deserves further study.

The ice cloud bulk single-scattering properties are parameterized in terms of the effective particle size of the aforementioned 34 size distributions. The effective size is defined as the 1.5 times of the ratio of average volume of ice crystal particles to their average projected area. Fig. 2 shows the mean single-scattering properties (extinction efficiency, absorption efficiency, and asymmetry factor) for four effective sizes of ice clouds ($D_e = 10, 30, 50,$ and 80 μm) within the spectral range 750–1250 cm^{-1}. The calculations shown in Fig. 2 were performed using the parameterization scheme developed by Yang *et al.* [25] for the optical properties of ice crystals. The mean extinction efficiency of ice crystals depends strongly on wavenumber, particularly, for small particle sizes. The extinction minimum at 950 cm^{-1} becomes more pronounced with decreasing particle size, and corresponds to the Christiansen band of ice [36], [37]. For large particle sizes ($D_e = 50$ and 80 μm), the spectral variation of the extinction efficiency is relatively smooth. The total extinction efficiencies of ice crystals (i.e., the sum of scattering and absorption effects) in the 1000–1250-cm^{-1} spectral region are nearly independent of effective particle size when the sizes are large, a characteristic that is useful for the retrieval of ice cloud optical thickness.

The bulk absorption efficiency is related to the imaginary part of the complex refractive index of ice. In addition, the absorption of ice crystals depends on wavenumber and the effective particle size. The absorption efficiency varies with wavenumber in the 750–1000-cm^{-1} spectral region, particularly for small effective particle sizes. This feature is useful for determining the effective size of ice crystals from high-resolution IR atmospheric spectral measurements. The asymmetry factor increases with effective particle size in the IR spectral region, implying that the scattering of the incident radiation by ice crystals is typically in the forward direction.

For water clouds, the bulk single scattering properties were calculated using the Lorenz–Mie theory [26], and assuming Gamma particle size distributions. The scattering properties of spherical particles have been extensively discussed by Hansen and Travis [38].

B. Numerical Simulation of Upwelling Infrared Radiances at Aircraft Level

Clear-sky (noncloudy) monochromatic atmospheric molecular absorption optical thicknesses are computed from a line-by-line (LBL) radiative transfer model originally developed by Chou and Kouvaris [39]. For the present application, the atmosphere is divided into one hundred layers between the surface and an altitude of 20 km. Rawinsonde profiles provide atmospheric temperature, pressure, density and water vapor; the spectral line parameters of atmospheric gases are from HITRAN 2000 [40] (note that the term "HITRAN" is an acronym for high-resolution transmission molecular absorption database); and the Voigt line shape [41] that accounts for both pressure and temperature broadening effects is used for computing the line absorption of atmospheric gas molecules. The continuum absorption of water vapor and other gases within 750–1250 cm^{-1} are calculated using the CKD-2.4 model [42]. To facilitate the comparison of the model simulation with the high-resolution interferometer sounder (HIS) measurement, as needed in the implementation of the retrieval technique, the monochromatic total optical thicknesses of atmospheric gases at every level are convolved with the instrumental response function.

The upwelling atmospheric radiative spectrum under cloudy conditions at the aircraft altitude (20 km) is then computed in terms of brightness temperature by combining the clear-sky optical thickness from the LBL code and the discrete ordinates method radiative transfer (DISORT) [43]. Clouds are simulated by adding an optical thickness, single-scattering albedo, and scattering phase function for a model atmospheric layer. The DISORT method is implemented with 16 streams used in the calculations. The spectral interval is 0.2 cm^{-1}. The Legendre coefficients of the phase functions are derived from Hu's algorithm [44] that properly accounts for the truncation of the strong forward peak.

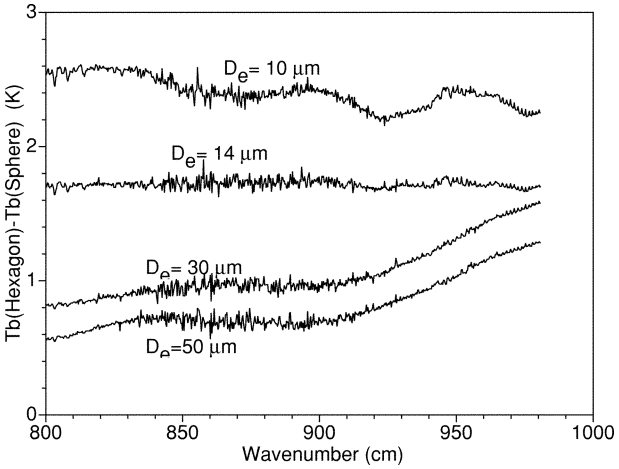

Fig. 3. Shown are the differences in simulated upwelling brightness temperatures calculated for hexagonal ice crystals and spherical particles as a function of wavenumber for four effective sizes of ice clouds, but for a fixed cloud optical thickness of 1. Two sets of spectral brightness temperatures are calculated as a function of wavenumber based on the single-scattering properties for four particle size distributions of both ice spheres and the hexagonal ice crystals. The two sets of resulting brightness temperature spectra for each size distribution are then differenced. The atmospheric profiles are provided from a nearby rawinsonde. The surface skin temperature is 267.6 K and the cloud altitude is 7 km.

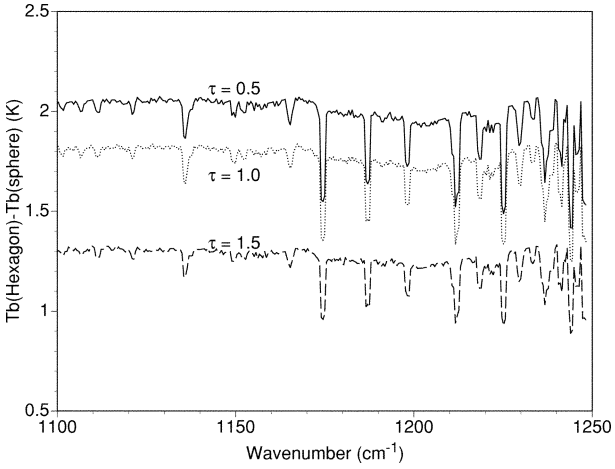

Fig. 4. Shown are the differences in simulated upwelling brightness temperature spectra computed for hexagonal ice crystals and spherical particles. The brightness temperature differences are presented as a function of wavenumber for three cloud optical thicknesses. The effective particle size is fixed at 14 μm.

C. Effect of Ice Crystal Nonsphericity

The significance of ice crystal nonsphericity in the retrieval of cloud optical thickness at Vis and NIR wavelengths has been discussed by Mishchenko *et al.* [45], [46], Takano *et al.* [47] and references cited therein. Here, we investigate the effect of ice crystal nonsphericity on high-resolution IR spectral radiance simulations. Based on the single-scattering properties for the same size distributions of both hexagonal ice crystals and the corresponding equivalent ice spheres, two sets of spectral-dependent brightness temperatures are calculated as functions of wavenumber. The visible optical thickness is fixed at 1 for these simulations. The two sets of resulting brightness temperatures for each size distribution are then differenced, with the results shown in Fig. 3 for the 800–1000-cm^{-1} spectral region. The brightness temperatures for spherical ice particles are 0.5–2.6 K lower than that for nonspherical particles. This is caused by the overestimation of the absorption and extinction efficiencies that occurs with the use of the spherical approximation [37].

The previous results were obtained for a fixed optical thickness. Similar calculations can be made in which the particle size is fixed but the optical thickness varies. The results in Fig. 4 show the difference in spectral brightness temperatures calculated for three values of optical thickness within the 1100–1250-cm^{-1} spectral region, but for these simulations the effective particle size is fixed at 14 μm. The brightness temperatures for spherical ice particles are 1–2 K lower than that for nonspherical particles, depending on the optical thickness of the cloud.

Figs. 3 and 4 demonstrate that the nonsphericity of ice crystals can have a significant effect on the optical properties inferred from IR measurements and that the spherical particle approximation for inferring ice cloud properties may result in an overestimatation of the optical thickness and an inaccurate retrieval of effective particle size.

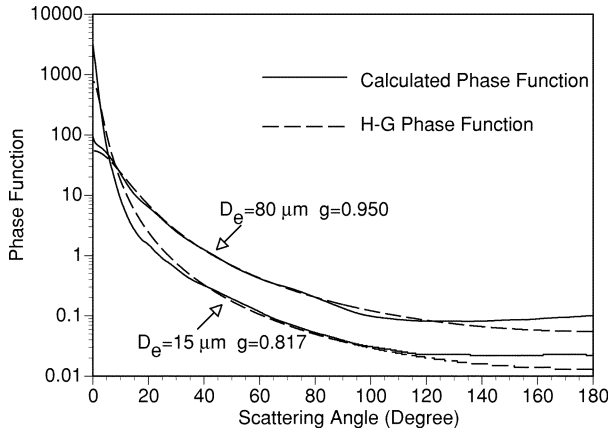

Fig. 5. Comparison of the bulk phase function calculated using nonspherical ice habits (droxtals and hexagonal columns) with a Henyey–Greenstein phase function for two effective particle sizes.

D. Errors Associated With the Use of Henyey–Greenstein Phase Function

The impact of the nonspherical ice particles on optical properties raises the question of using a simplified form of the phase function in the radiative transfer simulations. Due to its simplicity and efficiency, the H–G phase function is widely used in the IR radiative transfer calculations as an approximation for describing the phase function of cloud particles. In this section we compare the H–G phase function with the more complex phase function calculated for the more realistic ice crystals from the FDTD and an improved geometric optics methods. The phase functions for individual crystals are averaged over the 34 ice cloud size distributions as discussed previously. For two different size distributions, Fig. 5 shows a comparison between the actual phase functions derived for hexagonal ice crystals and the H–G phase functions derived using the asymmetry factor obtained for each distribution. Compared with the nonspherical ice crystal phase functions, the H–G phase function is smoother and smaller in magnitude in both the forward- and back-scattering directions.

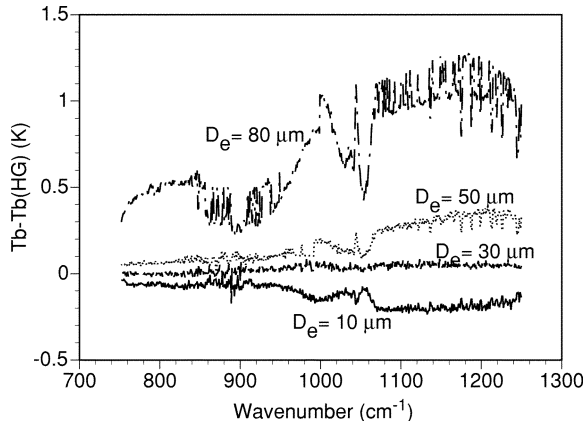

Fig. 6. Shown are the differences in the simulated spectral brightness temperatures from use of the actual phase function derived for nonspherical crystals and the simplified H–G phase function in the radiative transfer calculations. Results are shown for simulations of clouds having four effective particle sizes (10, 30, 50, and 80 μm). The calculations are performed at the aircraft altitude (20 km) and assume the US standard atmospheric model; a surface skin temperature of Ts $=$ 288.1 K; a cloud altitude of 10 km, and an optical thickness $\tau = 1$.

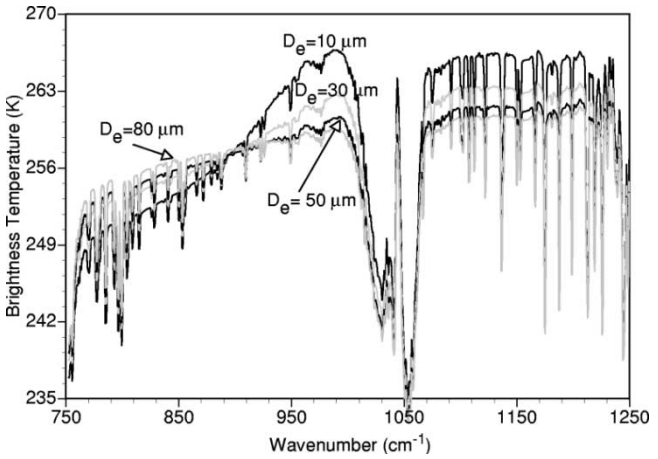

Fig. 7. Shown are the spectral brightness temperatures at the aircraft level (20 km) as a function of wavenumber for four effective particle sizes (10, 30, 50, and 80 μm). The calculations assume the US standard atmospheric model, a surface skin temperature of 288.1 K, a cloud altitude of 10 km, and an optical thickness $\tau = 1$.

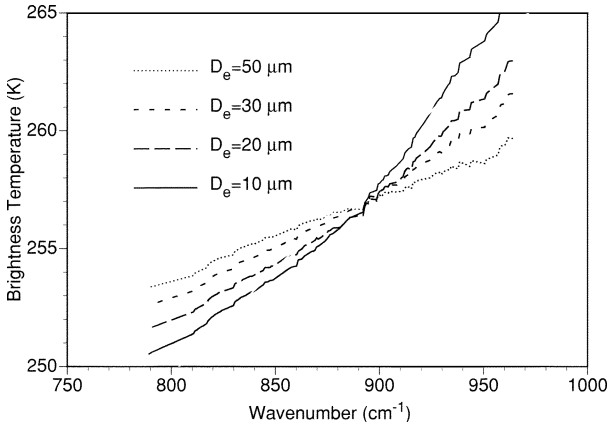

Fig. 8. For the spectral region between 790–960 cm^{-1}, the absorption lines between 790–960 cm^{-1} are removed and the resulting window brightness temperatures are interpolated across the gaps. This process more clearly shows how the slope of the observed spectral brightness temperature, with respect to wavenumber, depends upon the effective particle size.

Fig. 6 shows the differences in the simulated spectral brightness temperatures (converted from the upward spectral flux) at the aircraft level (20 km) between the results derived using the actual phase function derived for nonspherical crystals and the H–G phase function. The brightness temperature using the derived phase function is a little greater than that of the H–G phase function in most cases. The forward scattering of the nonspherical particle phase functions is usually larger than that of the H–G phase function. The largest differences occur at wavenumbers where strong scattering occurs (1000–1300 cm^{-1}) for large particle effective sizes. For small particle sizes, the difference between the two phase functions is much less, with brightness temperatures generally differing by less than 0.4 K. This may be due to the offset of the different phase functions within 0° to 90°. For clouds containing larger ice crystals with a large value of the asymmetry factor, the brightness temperature difference can be more than 1 K. The modified H–G phase function, such as the double H–G phase function, may offer a better result.

III. Sensitivity Study and Error Analysis

In this section, we present the physical basis of the retrieval technique by investigating the sensitivity of high spectral resolution IR brightness temperatures to the effective particle size and optical thickness. As this knowledge will later be used to derive the cloud properties from HIS radiances, we have used an observer altitude of 20 km, the cruising altitude of the ER-2 aircraft, in the upwelling radiance calculations. We also investigate the influence of the atmospheric profiles and the inaccuracies in the cloud temperature and surface skin temperature on the retrieval results.

A. Sensitivity of IR Radiance to Effective Particle Size

Fig. 7 illustrates the sensitivity of the upwelling brightness temperature spectrum to the ice cloud effective particle size. The spectral brightness temperatures between atmospheric molecular absorption lines (i.e., the atmospheric windows) increase with wavenumber within the 760–1000-cm^{-1} region because ice crystal absorption decreases with wavenumber. However, the absorption is also size-dependent. The ice clouds with smaller effective sizes absorb more radiance from below the cloud at smaller wavenumbers, leading to a steeper slope in brightness temperature for clouds composed of small particles than for large particles.

From the brightness temperature at atmospheric window wavenumbers, ignoring the strong absorption wavenumbers to remove the absorption lines within 790–960 cm^{-1} and interpolating the brightness temperatures across the gaps, we notice that there is a considerable sensitivity in the slope of the observed brightness temperature to the effective particle size (see Fig. 8). This sensitivity, in which the slope in brightness temperature increases with decreasing particle size, forms the basis for the inference of effective particle size. We calculate the brightness temperature at the atmospheric windows in the 790–960-cm^{-1} region, and obtain the slope for a range of different effective particle sizes and values of optical thickness.

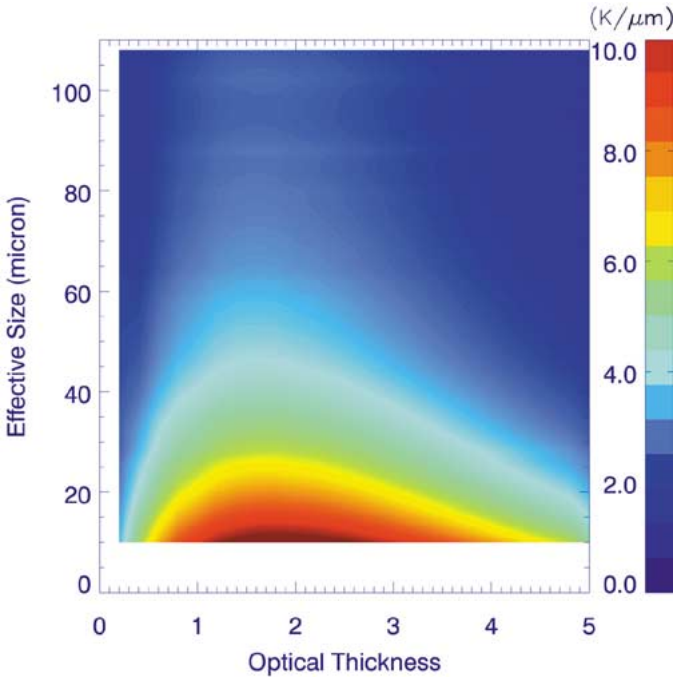

Fig. 9. As in Fig. 8, but extended to include both the effect of optical thickness and particle size on the slope of the spectral brightness temperatures and wavenumber between 790–960 cm^{-1}.

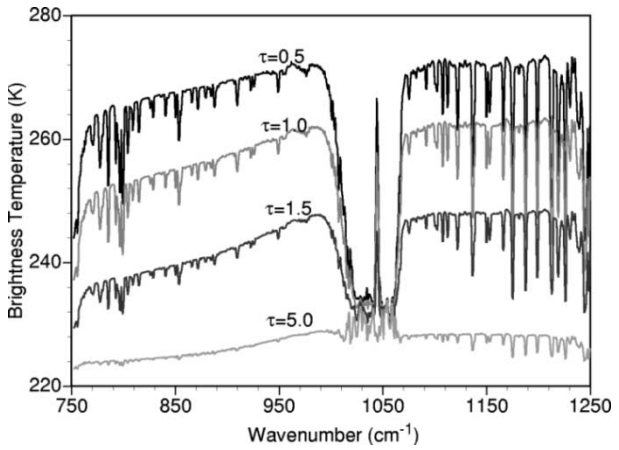

Fig. 10. Same as Fig. 7, but for the sensitivity of spectral brightness temperature to the cloud optical thickness. The assumed effective particle size is fixed at 30 μm.

As shown in Fig. 9, the variation of the slope is most sensitive to clouds having lower values of effective particle size and optical thicknesses between 0.4 and 4. For example, for a cloud having an optical thickness of 1, the slope decreases from 9–2 K/μm as the effective particle size increases from 10–80 μm.

B. Sensitivity of IR Radiance to Optical Thickness of Clouds

Fig. 10 shows simulated upwelling brightness temperature at a 20-km altitude for four values of optical thickness and a fixed effective particle size of 30 μm. The brightness temperature varies with wavenumber between 750–1000 cm^{-1} for small to moderate optical thicknesses. As shown in Fig. 10, the brightness temperature decreases more than 40 K as the optical thickness increases from 0.5–5. For optically thick ice clouds (optical thickness larger than 5), the brightness temperature has less dependence on wavenumber.

C. Error Analysis

The brightness temperature discretization in Fig. 9 is 0.5 K/μm. If we assume that the minimum measurable temperature difference is 1 K, the effective particle size cannot be accurately retrieved in the case when if the variation of brightness temperature difference between 950 and 790 cm^{-1} is less than 1 K due to the variation of the effective particle size. Further theoretical error analyses suggests that, for a threshold of 0.5 K/μm, the maximum retrievable effective size can be no larger than 80 μm with an uncertainty of 10 μm. The uncertainty decreases to about 2 μm when the effective size is 10 μm. Similarly, the maximum retrievable optical thickness is approximately 8 with an uncertainty of 1. For the case of a visible optical thickness of 1, the uncertainty decreases to less than 0.1.

In the IR spectrum, the surface skin temperature, cloud temperature and atmospheric profile contributed significantly to the top of atmosphere radiance. Hence, in the remainder of the section, we study the effects of uncertainties in surface and cloud temperature to retrieval results. We also investigate the sensitivity for different atmospheric profiles.

D. Effects of Surface and Cloud Temperature on Retrieval Accuracy

In this section, we analyze the effects of inaccurate specification of surface and cloud temperature on the accuracy of the inferred microphysical and optical properties. Cloud-top pressure or temperature may be inferred by methods such as the CO_2 slicing method [48] or by the minimum local emissivity variance (MLEV) method [49]. The MLEV algorithm uses a physical approach in which the local spectral variances of cloud emissivity are calculated for a number of assumed cloud pressures. The optimal cloud emissivity spectrum is that which has the minimum local emissivity variance among the retrieved emissivity spectra associated with different assumed cloud pressures. This technique is based on the observation that the absorption, reflection, and scattering processes of clouds exhibit relatively limited localized spectral emissivity structure in the 750–1250-cm^{-1} spectral region. Any retrieved cloud emissivity that exhibits spectral variation similar to that of carbon dioxide and water vapor absorption is indicative of an incorrect specification of cloud pressure level and its associated spectral emissivity. MLEV analysis shows that cloud pressure root mean square errors for a single layer cloud with an effective cloud emissivity greater than 0.1 are $\sim$ 30, $\sim$ 10, and $\sim$ 50 hPa, for high, middle, and low clouds, respectively.

Errors in the assigned cloud pressure and its corresponding temperature will affect the retrieval of optical thickness. Fig. 11 shows the predicted error in the retrieved optical thickness as a function of cloud temperature error. The error of cloud temperature is assumed to be within $\pm$7 K, corresponding to the variation of temperature at a cloud altitude of 10 $\pm$ 1 km. A lower-than-actual cloud temperature will result in an overestimate of the optical thickness, while a higher-than-actual cloud temperature will lead to an underestimate of optical thickness. The impact of the cloud temperature error is more pronounced for optically thick ice clouds than for optically thin ice clouds. Generally speaking, the error in the retrieved optical thickness is less than 10% if the cloud temperature is within $\pm$5 K of the true temperature and the cloud optical thickness is less than 2.

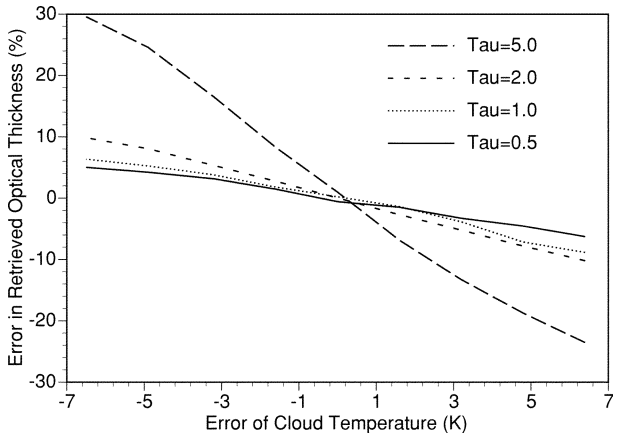

Fig. 11. Errors in retrieved optical thickness resulting from an error in cloud temperature for four optical thicknesses. The ice cloud has an effective particle size of 25 μm. The actual cloud temperature is assumed to be 223.3 K, but varies from 229.7–216.8 K.

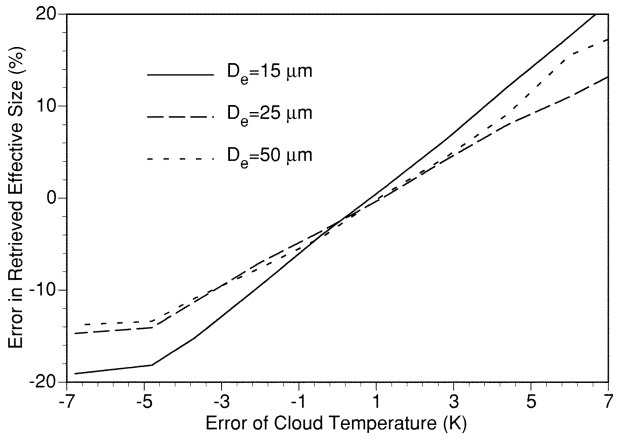

Fig. 12. Errors in retrieved effective size to the error of cloud temperature for three effective particle sizes. The ice cloud has an optical thickness of 1.

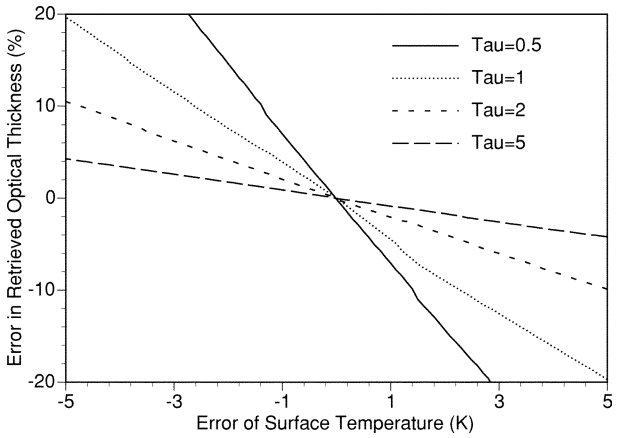

Fig. 13. Errors in retrieved optical thickness resulting from an error in surface skin temperature for four cloud optical thicknesses. The ice cloud has an effective particle size of 25 μm and is located at an altitude of 10 km.

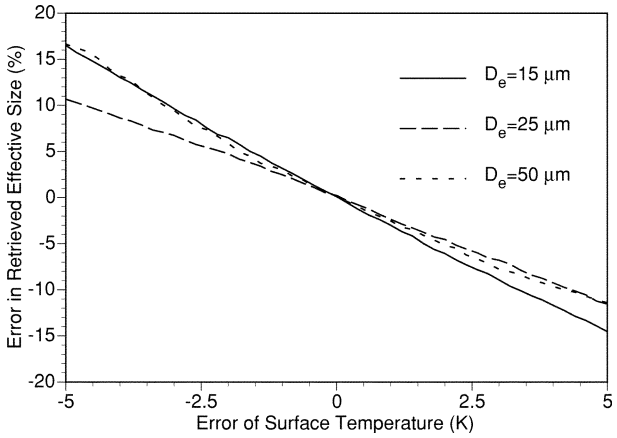

Fig. 14. Errors in retrieved effective size caused by an error in surface skin temperature for three effective particle sizes. The cloud optical thickness is constant at 1, and the cloud altitude is 10 km.

Fig. 12 shows the relationship between the retrieved effective particle size and the cloud temperature error. Different cloud temperatures result in different brightness temperature slopes, and thus lead to effective particle size retrieval errors. The error is within $\pm 15\%$ if the cloud temperature error is within ± 5 K.

Fig. 13 shows the error in the retrieved optical thickness as a function of surface skin temperature error. An error in the surface skin temperature has a pronounced influence on the retrieval of optical thickness if the cloud is optically thin, because the upwelling radiation is primarily from the surface, with some modest attenuation by the atmosphere and clouds. For very thick clouds, an error in the surface skin temperature has little influence on the retrieved optical thickness. For the retrieval accuracy of optical thickness (Fig. 13) to be better than 10%, the surface skin temperature error should be less than ± 2.5 K. Fig. 14 shows the dependence of the retrieved error in effective particle size on the error in surface skin temperature. Compared to the results in Fig. 13, an error in surface skin temperature (Fig. 14) has less influence on the effective particle size than on the optical thickness, because the variation of the surface skin temperature does not change as much with the slope of brightness temperature between 790–960 cm^{-1}. If the error of surface skin temperature is within ± 2.5 K, the error of retrieved effective particle size will be within $\pm 5\%$.

E. Effect of the Atmospheric Profiles

We now investigate the sensitivity of the brightness temperature to different regional average atmospheric profiles by calculating the brightness temperature difference between clear-sky and cloudy radiance, defined as the cloud forcing. Fig. 15 shows the cloud forcing for both a climatological tropical (TRO) and subarctic winter (AW) atmosphere for two assumed values of cloud optical thickness. We assume that the surface skin temperature is the same as the atmospheric temperature of the lowest layer, i.e., 300 K (tropical) and 257.1 K (subarctic winter). Because the upwelling radiances (and hence brightness temperatures) for the subarctic winter atmosphere are much lower than that of the tropical atmosphere, the sensitivity decreases for the subarctic winter atmosphere relative to a warmer tropical atmosphere. Even for the subarctic winter atmopsheric model, however, the variation of cloud forcing can still be more than 20 K when the optical thickness increases from 0.5–2. Thus, the IR spectra still contains sufficient information in these conditions from which the properties of ice clouds can be inferred using the simultaneous retrieval technique.

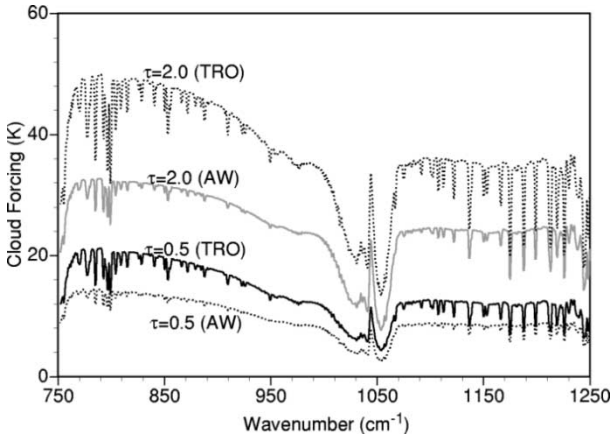

Fig. 15. Sensitivity of cloud forcing (brightness temperature difference between clear and cloudy sky) to the atmospheric model for two cloud optical thicknesses.

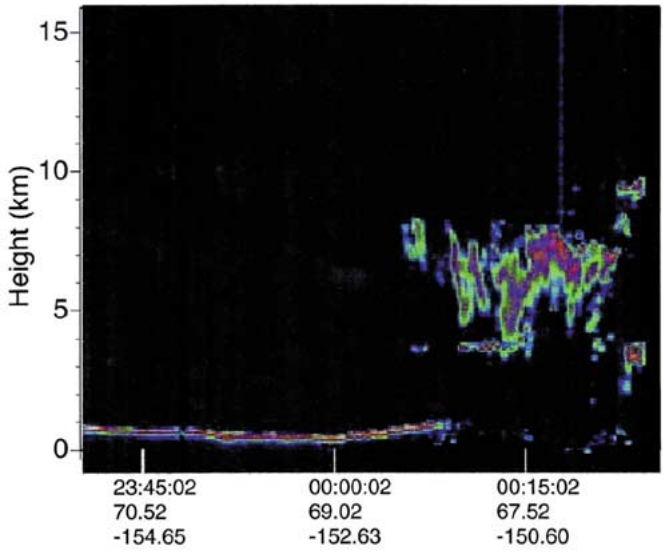

Fig. 16. CLS imagery providing information on cloud heights and boundaries. The scanning times, given in the format HH : MM : SS, used in this paper are 00 : 05 : 23 for the water cloud data, and 00 : 17 : 01 for ice cloud data. Scanning locations in degrees latitude and longitude are given below the time values.

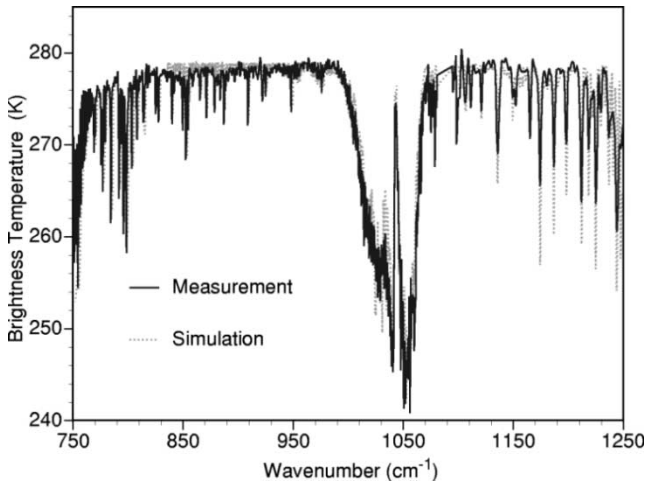

Fig. 17. Observed and simulated IR upwelling spectra under clear-sky conditions for May 23, 1998, 00 : 09 : 04 UT; surface skin temperature is 279 K.

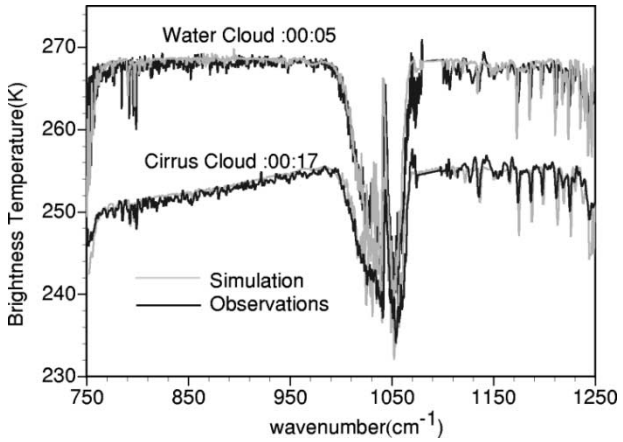

Fig. 18. Observed and simulated upwelling IR spectra for ice and water cloud conditions (the number in the figure is given in the format HH : MM UT on May 23, 1998).

IV. Inference of Ice Cloud Microphysical and Optical Properties

A. Simultaneous Retrieval Algorithm

An understanding of the above dependence of the upwelling radiance to cloud properties leads us to the following methodology for simultaneous retrieval of effective particle size and optical thickness.

First, the clear-sky atmospheric optical thickness profile is calculated with the LBL radiative transfer code. Given the height and temperature of an ice cloud, a series of spectral radiances are simulated using DISORT for a range of cloud effective particle sizes and optical thicknesses, and the precalculated cloud optical properties discussed in Section II-A. By matching the slope of the simulated brightness temperature in the 790–960-cm^{-1} band to the observed spectrum, the effective particle size of the ice cloud D_e can be estimated (note that, at this initial stage, a first-guess optical thickness τ is used). Then, the optical thickness is derived by comparing the observed spectrum to the simulations in 1100–1250-cm^{-1} band with the values of D_e determined in the previous step. The final particle size and optical thickness are obtained by iteration until the differences are minimized between the observed and simulated IR spectrum. The best fit retrieval is reached when the differences (variances) between the model simulation and measurement within the two bands are minimal.

In the following section, we apply the simultaneous retrieval algorithm outlined above to HIS data collected from two field experiments.

B. Case Study 1: Fire-ACE Experiment

During FIRE-ACE [50], upwelling spectral radiances were observed by the HIS instrument onboard the ER-2 aircraft from an altitude of 20 km. HIS data from band 1 (750–1080 cm^{-1}) and band 2 (1100–1250 cm^{-1}) were selected for analysis between 2345 UT and 0020 UT on May 22–23, 1998. This period provides example observations for water clouds (before 0007 UT), clear sky (0007–0010 UT), and high ice clouds (after 0010 UT). The data were recorded over an area in Alaska near 67.52°N, 150.60°W. Fig. 16 shows the Cloud Lidar System (CLS) imagery for this period, which provides information on the cloud-top altitude [51] and was used together with a MODIS

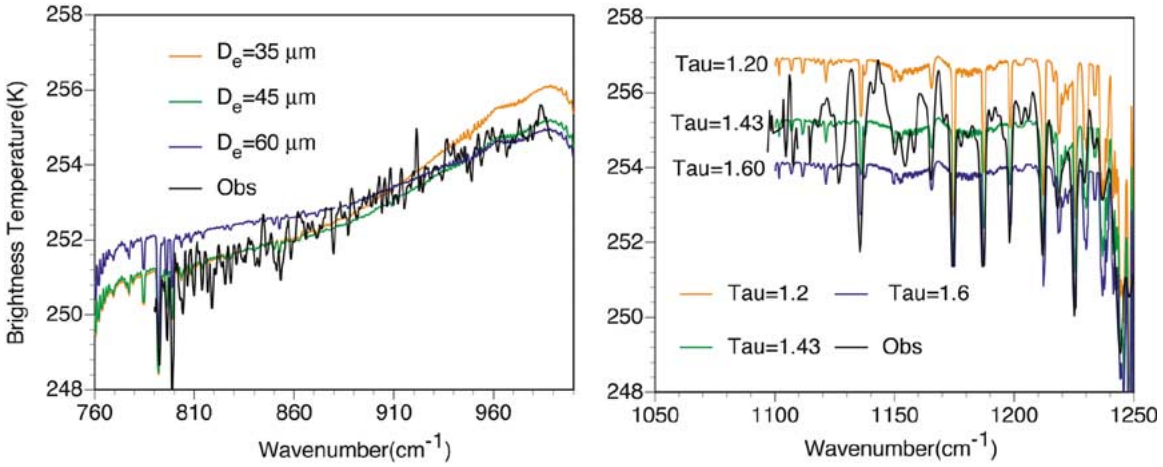

Fig. 19. Simultaneous retrieval of the effective size and optical thickness of ice clouds from HIS spectra. (a) Brightness temperature versus particle size assuming $\tau = 1.43$. (b) Brightness temperature versus optical thickness assuming $D_e = 45\ \mu$m. Date: May 23, 1998, 00:17:01 UT. The surface skin temperature is 267.6 K, and the cloud altitude is 7.0 km.

Airborne Simulator (MAS) image (not shown here) to discriminate between clear-sky, water cloud, and ice cloud conditions.

The HIS brightness temperature spectrum for clear sky (0009 UT) is shown in Fig. 17, while those for water clouds (0005 UT) and high ice clouds (0017 UT) are shown in Fig. 18. Also plotted on these two figures are the best fit simulated radiances that were generated from temperature, pressure and relative humidity data from a nearby rawinsonde at 2324 UT on May 22, 1998, together with cloud properties determined using our retrieval technique.

Fig. 18 demonstrates that the observed spectral signature of the ice cloud is quite different from that of the water cloud. The brightness temperature of the ice cloud increases with wavenumber over the 750–1000-cm^{-1} region. This expected result, as previously mentioned, is due to the spectral variation of the absorption of ice crystals.

Fig. 19 illustrates the process of matching the simulated and observed brightness temperatures by varying (and thus, when the brightness temperatures match, retrieving) the cloud properties in the simulations. The left panel of Fig. 19 shows comparisons of the observed HIS spectrum (solid black curve) with simulated brightness temperatures for a number of trial effective particle sizes $D_e = 35,\ 45,$ and 60 μm and a first-guess optical thickness $\tau = 1.43$, within the 760–1000-cm^{-1} band. The right panel of Fig. 19 shows brightness temperatures for the best matched effective particle size $D_e = 45.0\ \mu$m (as determined from the previous step as illustrated in left panel of Fig. 19) with trial optical thickness values $\tau = 1.2$, 1.43, and 1.6 within the 1100–1250-cm^{-1} band). The effective particle size is inferred by fitting a line between 790–960 cm^{-1}. The resultant values of the effective particle size and optical thickness in this case are 45 μm and 1.43, respectively.

C. Case Study 2: SUCCESS Experiment (Small-Particle Case)

Smith *et al.* [2] reported a strong absorption signature of very small ice cloud particles during SUCCESS in 1996. Fig. 20 shows the HIS spectrum collected from the ER-2 during an overflight of a jet aircraft contrail, which generally consists of very small particles. The best fit simulated spectral brightness temperatures shown are simulations for an ice cloud model based solely on droxtals with an effective particle size of 12.5 μm (or an effective radius of 6.25 μm), and an optical thickness of 1.60. The simulation generally agrees well with the observed spectrum (except at 990 cm^{-1}, probably due to the residual effect of an imperfect ozone concentration profile) and indicates that the droxtal crystal habit seems to be a realistic approximation for small ice particles. Chung *et al.* [14] calculated the spectrum for this case by assuming that ice clouds are composed of spherical ice particles with an assumed Gamma size distribution. The retrieved effective radius (7.35 μm) and IWP (6.85 g/m^2) corresponds to an optical thickness of 1.5 in that study. The present optical thickness is close to Chung's result, but the effective particle size inferred in this paper is a little smaller. The differences are due to the more complex ice habit (droxtal) used in the present retrieval. A droxtal with the same maximum dimension will have smaller effective size than the ice sphere. Thus, the retrieved effective size is slightly lower by assuming the droxtal instead of sphere.

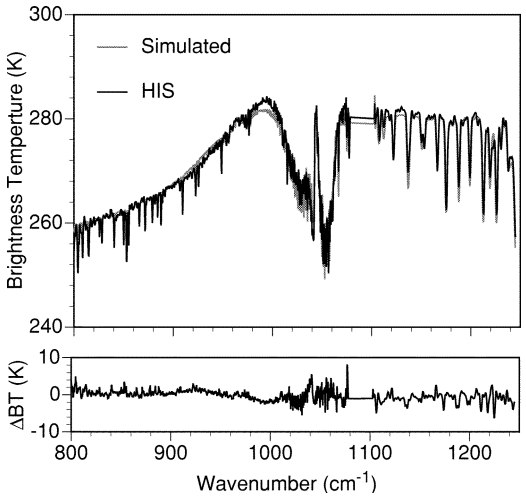

Fig. 20. Comparison of observed and simulated upwelling IR spectra at 20 km altitude for a jet contrail composed of primarily small ice particles ($D_e = 12.5\ \mu$m, $\tau = 1.6$).

V. Summary

Within the 750–1000-cm^{-1} spectral region, the slope of brightness temperature is sensitive to ice crystal effective particle size, particularly for small particle sizes. At wavenumbers between 1100 and 1250 cm^{-1}, the spectrum is more sensitive to the optical thickness than to particle size. Thus, using the terrestrial window information within the 750–1250-cm^{-1} spectral band, we can infer the optical thickness and effective particle size for ice clouds simultaneously.

An error analysis is performed to investigate the uncertainty of the retrieved optical thickness and effective particle size. The error for retrieving particle size in conjunction with an uncertainty of 5 K in cloud temperature, or a surface temperature uncertainty of 2.5 K, is less than 15%. The corresponding error in the uncertainty of optical thickness is within 5% to 20%, depending on the value of cloud optical thickness.

The maximum effective particle size that may be retrieved with the present approach (i.e., an upper limit) is 80 μm with an uncertainty of approximately 10 μm at $D_e = 80$ μm, and about 2-μm uncertainty at $D_e = 10$ μm. The maximum retrievable optical thickness is approximately 8 with an uncertainty of 1. For the case of optical thickness 1, the uncertainty decreases to less than 0.1.

The applicability of the technique is demonstrated using the aircraft-based HIS data from the SUCCESS experiment in 1996 and FIRE-ACE in 1998. The IR brightness temperature simulations corresponding to the simultaneous retrieval of cloud optical thickness and particle effective size for two cases with particle sizes of 45 and 12.5 μm yield a reasonable fit to the observed spectra. Spectral temperature differences of ~ 4 K and > 20 K (derived from the slope of the spectral brightness temperatures at wavenumbers between 790–960 cm^{-1}) further demonstrate that the forward modeling of cloudy measurements and retrieval algorithm are capable of obtaining reliable cloud properties. A further cloud modeling study and retrieval validation using spaceborne and active cloud measurements, and *in situ* measurements may enhance our ability to refine this technique.

References

[1] D. K. Lynch, K. Sassen, D. O. Starr, and G. Stephens, Eds., *Cirrus*. New York: Oxford Univ. Press, 2002.

[2] W. L. Smith, S. Ackerman, H. Revercomb, H. Huang, D. H. DeSlover, W. Feltz, L. Gumley, and A. Collard, "Infrared spectral absorption of nearly invisible cirrus clouds," *Geophys. Res. Lett.*, vol. 25, pp. 1137–1140, 1998.

[3] G. L. Stephens, S. C. Tsay, and P. W. Flatau, "The relevance of microphysical and radiative properties of cirrus clouds to climate and clime feedback," *J. Atmos. Sci.*, vol. 47, pp. 1742–1753, 1990.

[4] K. N. Liou, "Influence of cirrus clouds on weather and climate processes: A global perspective," *Mon. Weather Rev.*, vol. 114, pp. 1167–1199, 1986.

[5] T. Nakajima and M. D. King, "Determination of the optical thickness and effective particle radius of clouds from reflected solar radiation measurements. Part I: Theory," *J. Atmos. Sci*, vol. 47, pp. 1878–1893, 1990.

[6] M. D. King, W. P. Menzel, Y. J. Kaufman, D. Tanré, B. C. Gao, S. Platnick, S. A. Ackerman, L. A. Remer, R. Pincus, and P. A. Hubanks, "Cloud and aerosol properties, precipitable water, and profiles of temperature and humidity from MODIS," *IEEE Trans. Geosci. Remote Sensing*, vol. 41, pp. 442–458, Feb. 2003.

[7] S. Platnick, M. D. King, S. A. Ackerman, W. P. Menzel, B. A. Baum, J. C. Riédi, and R. A. Frey, "The MODIS cloud products: Algorithms and examples from Terra," *IEEE Trans. Geosci. Remote Sens.*, vol. 41, pp. 459–473, Feb. 2003.

[8] C. J. Stubenrauch, R. Holz, A. Chedin, D. L. Mitchell, and A. J. Baran, "Retrieval of cirrus ice crystal sizes from 8.3 and 11.1 μm emissivities determined by the improved initialization inversion of TIROS-N operational vertical sounder observations," *J Geophys Res.*, vol. 104, pp. 793–808, 1999.

[9] P. Zuidema, "Convective clouds over the Bay of Bengal," *Mon. Weather Rev.*, vol. 131, pp. 780–798, 2003.

[10] W. L. Smith, D. K. Zhou, F. W. Harrison, H. E. Revercomb, A. M. Larar, H.-L. Huang, and B. Huang, "2000: Hyperspectral remote sensing of atmospheric profiles from satellites and aircraft," in *Proc. SPIE Hyperspectral Remote Sensing of the Land and Atmosphere Conf.*, W. L. Smith and Y. Yasuoka, Eds., Oct. 9–12, 2000, pp. 94–102.

[11] H.-L. Huang, H. E. Revercomb, J. Thom, P. B. Antonelli, B. Osborne, D. Tobin, R. Knuteson, R. Garcia, S. Dutcher, J. Li, and W. L. Smith, "2000: Geostationary imaging FTS (GIFTS) data processing: Measurement simulation and compression," in *Proc. SPIE Conf. Hyperspectral Remote Sensing of the Land and Atmosphere*, W. L. Smith and Y. Yasuoka, Eds., Oct. 9–12, 2000, pp. 103–114.

[12] R. J. Glumb, D. C. Jordan, and P. Mantica, "2002: Development of the Crosstrack Infrared Sounder (CrIS) sensor design," in *Proc. 9th SPIE Infrared Spaceborne Remote Sensing Conf.*, vol. 4486, M. Strojnik and B. F. Andresen, Eds., pp. 411–424.

[13] S. Ou, K. N. Liou, P. Yang, P. Rolland, T. R. Caudill, J. Lisowski, and B. Morrison, "Airborne retrieval of cirrus cloud optical and microphysical properties using ARES 5.1–5.3 μm channel data," *J. Geophys. Res.*, vol. 103, pp. 23 231–23 242, 1998.

[14] S. Chung, S. Ackerman, P. F. Van Delst, and W. P. Menzel, "Model calculations and interferometer measurements of ice-clouds characteristics," *J. Appl. Meteorol.*, vol. 39, pp. 634–644, 2000.

[15] S. A. Ackerman, W. L. Smith, J. D. Spinhirne, and H. E. Revercomb, "The 27–28 october 1986 far-IRE IFO cirrus case study: Spectral properties of cirrus clouds in the 8–12 μm window," *Mon. Weather Rev.*, vol. 118, pp. 2377–2388, 1990.

[16] R. J. Bantges, J. E. Russell, and J. D. Haigh, "Cirrus cloud top-of-atmosphere radiance spectra in the thermal infrared," *J. Quant. Spectrosc. Radiat. Transf.*, vol. 63, pp. 487–498, 1999.

[17] D. H. DeSlover, W. L. Smith, P. K. Piironen, and E. W. Eloranta, "A methodology for measuring cirrus cloud visible-to-infrared spectral optical thickness ratios," *J. Atmos. Oceanic Technol.*, vol. 16, pp. 251–262, 1999.

[18] B. H. K. Kahn, A. Eldering, F. W. Irion, F. P. Mills, B. Sen, and M. R. Gunson, "Cloud identification in atmospheric trace molecule spectroscopy infrared occultation measurements," *Appl. Opt.*, vol. 41, pp. 2768–2780, 2002.

[19] A. Eldering, F. W. Irion, A. Y. Chang, M. R. Gunson, F. P. Mills, and H. M. Steele, "Vertical profiles of aerosol volume from high-spectral-resolution infrared transmission measurements," *Appl. Opt.*, vol. 40, pp. 3082–3090, 2001.

[20] C. Rathke and J. Fischer, "Retrieval of cloud microphysical properties from thermal infrared observations by a fast iterative radiance fitting method," *J. Atmos. Oceanic Technol.*, vol. 17, pp. 1509–1524, 2000.

[21] M. D. Chou, K. T. Lee, S. C. Tsay, and Q. Fu, "Parameterization for cloud longwave scattering for use in atmospheric models," *J. Climate*, vol. 12, pp. 159–169, 1999.

[22] A. J. Heymsfield and C. M. R. Platt, "A parameterization of the particle size spectrum of ice clouds in terms of the ambient temperature and the ice water content," *J. Atmos. Sci.*, vol. 41, pp. 846–855, 1984.

[23] A. J. Heymsfield and J. Iaquinta, "Cirrus crystal terminal velocities," *J. Atmos. Sci.*, vol. 5, pp. 916–938, 2000.

[24] P. Yang, B. A. Baum, A. J. Heymsfield, Y. X. Hu, H.-L. Huang, S.-C. Tsay, and S. Ackerman, "Single-scattering properties of droxtals," *J. Quant. Spectrosc. Radiat. Transf.*, vol. 79–80, pp. 1159–1169, 2003.

[25] P. Yang, B. C. Gao, B. A. Baum, Y. X. Hu, W. J. Wiscombe, S. C. Tsay, D. M. Winker, and S. L. Nasiri, "Radiative properties of cirrus clouds in the infrared (8–13 μm) spectral region," *J. Quant. Spectrosc. Radiat. Transf.*, vol. 70, pp. 473–504, 2001.

[26] P. Yang and K. N. Liou, "Finite-difference time domain method for light scattering by small ice crystals in three-dimensional space," *J. Opt. Soc. Amer.*, vol. A13, pp. 2072–2085, 1996.

[27] W. J. Wiscombe, "Improved Mie scattering algorithms," *Appl. Opt.*, vol. 19, pp. 1505–1509, 1980.

[28] Q. Fu, W. B. Sun, and P. Yang, "On modeling of scattering and absorption by cirrus nonspherical ice particles at thermal infrared wavelengths," *J. Atmos Sci.*, vol. 56, pp. 2937–2947, 1999.

[29] P. Yang and K. N. Liou, "Geometric-optics-integral-equation method for light scattering by nonspherical ice crystals," *Appl. Opt.*, vol. 35, pp. 6568–6584, 1996.

[30] P. Yang, B.-C. Gao, B. A. Baum, W. Wiscombe, M. I. Mischenko, D. M. Winker, and S. L. Nasiri, "Asymptotic solutions of optical properties of large particles with strong absorption," *Appl. Opt.*, vol. 40, pp. 1532–1547, 2001.

[31] Y. K. Lee, P. Yang, M. I. Mishchenko, B. A. Baum, Y. Hu, H.-L. Huang, W. J. Wiscombe, and A. J. Baran, "On the use of circular cylinders as surrogates for hexagonal pristine ice crystals in scattering calculations at infrared wavelengths," *Appl. Opt.*, vol. 42, pp. 2653–266, 2003.

[32] M. I. Mishchenko and L. D. Travis, "Capabilities and limitations of a current FORTRAN implementation of the T-matrix method for randomly oriented rotationally symmetric scatters," *J. Quant. Spectrosc. Radiat. Transf.*, vol. 60, pp. 309–324, 1998.

[33] Q. Fu, P. Yang, and W. B. Sun, "An accurate parameterization of the infrared radiative properties of cirrus clouds for climate models," *J. Climate*, vol. 25, pp. 2223–2237, 1998.

[34] D. L. Mitchell, S. K. Chai, Y. Liu, A. J. Heymsfeld, and Y. Dong, "Modeling cirrus clouds. Part I: Treatment of bimodal size spectra and case study analysis," *J. Atmos. Sci.*, vol. 53, pp. 2952–2966, 1996.

[35] Q. Fu and W. B. Sun, "Retrieval of cirrus particle sizes using a split-window technique: A sensitivity study," *J. Quant. Spectrosc. Radiat. Transfer*, vol. 70, pp. 725–736, 2001.

[36] W. P. Arnott, Y. Y. Dong, and D. J. Hallett, "Extinction efficiency in the infrared (2–18 μm) of laboratory ice clouds: Observations of scattering minimum in the Christiansen bands of ice," *Appl. Opt.*, vol. 34, pp. 541–551, 1995.

[37] P. Yang, K. N. Liou, and W. P. Arnott, "Extinction efficiency and single-scatttering albedo for laboratory and natural cirrus clouds," *J. Geophys. Res.*, vol. 103, pp. 825–835, 1997.

[38] J. E. Hansen and L. D. Travis, "Light scattering in planetary atmospheres," *Space Sci. Rev.*, vol. 16, pp. 527–610, 1974.

[39] M. D. Chou and L. Kouvaris, "Monochromatic calculations of atmospheric radiative transfer due to molecular line absorption," *J. Geophys. Res.*, vol. 91, pp. 4047–4055, 1986.

[40] L. S. Rothman *et al.*, "The HITRAN molecular spectroscopic database and HAWKS (HITRAN atmospheric Workstation): 1996 edition," *J. Quant. Spectrosc. Radiat. Transf.*, vol. 60, pp. 665–710, 1998.

[41] J. F. Kielkopf, "New approximation to the Voigt function with application to spectral line profiles," *J. Opt. Sci. Amer.*, vol. 63, pp. 987–995, 1973.

[42] D. C. Tobin, F. A. Best, S. A. Clough, R. G. Dedecker, R. G. Ellingson, R. K. Garcia, H. B. Howell, R. O. Knuteson, E. J. Mlawer, H. E. Revercomb, J. J. Short, P. F. W. van Delst, and V. P. Walden, "Downwelling spectral radiance observations at the SHEBA ice station: Water vapor continuum measurements from 17–26 μm," *J. Geophys. Res.*, vol. 104, pp. 2081–2092, 1999.

[43] K. Stamnes, S. C. Tsay, W. Wiscombe, and K. Jayaweera, "A numerically stable algorithm for discrete-ordinate-method radiative transfer in multiple scattering and emitting layered media," *Appl. Opt.*, vol. 27, pp. 2502–2509, 1988.

[44] Y. X. Hu, B. Wielicki, B. Lin, G. Gibson, S. C. Tsay, K. Stamnes, and T. Wong, "Delta-fit: A fast and accurate treatment of particle scattering phase functions with weighted singular-value decomposition least-square fitting," *J. Quant. Spectrosc. Radiat. Transf.*, vol. 65, pp. 681–690, 2000.

[45] *Light Scattering by Nonspherical Particles: Theory, Measurements, and Applications*, M. I. Mishchenko, J. W. Hovenier, and L. D. Travis, Eds., Academic, San Diego, CA, 2000.

[46] M. I. Mishchenko, W. B. Rossow, A. Macke, and A. A. Lacis, "Sensitivity of cirrus cloud albedo, bidirectional reflectance, and optical thickness retrieval to ice-particle shape," *J. Geophys. Res.*, vol. 101, pp. 16 973–16 985, 1996.

[47] Y. Takano, K. N. Liou, and P. Minnis, "The effects of small ice crystals on cirrus infrared radiative properties," *J. Atmos. Sci.*, vol. 49, pp. 1487–1493, 1992.

[48] D. P. Wylie and W. P. Menzel, "Eight years of global high cloud statistics using HIRS," *J. Climate*, vol. 12, pp. 170–184, 1999.

[49] H. L. Huang, W. L. Smith, J. Li, P. Antonelli, X. Wu, R. O. Knuteson, B. Huang, and B. J. Osborne, "Minimum local emissivity variance retrieval of cloud altitude and effective spectral emissivity simulation and initial verification," J. Appl. Meteorol., 2003, to be published.

[50] J. A. Curry, P. V. Hobbs, M. D. King, D. A. Randall, P. Minnis, G. A. Isaac, J. O. Pinto, T. Uttal, A. Bucholtz, D. G. Cripe, H. Gerber, C. W. Fairall, T. J. Garrett, J. Hudson, J. M. Intrieri, C. Jakob, T. Jensen, P. Lawson, D. Marcotte, L. Nguyen, P. Pilewskie, A. Rangno, D. C. Rogers, K. B. Strawbridge, F. P. J. Valero, A. G. Williams, and D. Wylie, "FIRE arctic clouds experiment," *Bull. Amer. Meteorol. Soc.*, vol. 81, pp. 5–29, 2000.

[51] J. D. Spinhirne and W. D. Hart, "Cirrus structure and radiative parameters from airborne lidar and spectral radiometer observations," *Mon. Weather Rev.*, vol. 118, pp. 2329–2343, 1990.

Hung-Lung Huang was borne in Taipei, Taiwan, R.O.C., in 1955. He received the B.S. degree in atmospheric science from National Taiwan University, Taipei, Taiwan, R.O.C., in 1979, and the M.S. and Ph.D. degrees in meteorology from the University of Wisconsin, Madison (UW), in 1986 and 1989, respectively.

From 1979 to 1984, he was a Satellite Meteorologist with the meteorological satellite ground station of the Taiwan Central Weather Bureau. Since 1989, he has been with Cooperative Institute for Meteorological Satellite Studies (CIMSS), UW as a Research Scientist, conducting remote sensing research in the areas of atmospheric sounding retrieval, information content analysis, satellite and aircraft high spectral resolution sounding instrument data processing, data compression, instrument design and performance analysis, and cloud property characterization. He is currently a Senior Scientist with CIMSS, a GIFTS Mission Scientist, and an Adjunct Professor with the Nanjing Institute of Meteorology, Nanjing, China.

Dr. Huang is a science council member of CIMSS, a council member of Space Science and Engineering Center of the UM, and is serving a two-year term as the Chair of Committee on Environmental Satellite Data Utilization of the National Research Council of the National Academies.

Ping Yang received the Ph.D. degree in meteorology from University of Utah, Salt Lake City, in 1995.

He is currently an Assistant Professor in the Department of Atmospheric Sciences, Texas A&M University, College Station. After graduation from the University of Utah, he remained with the university for two years, working as a Postdoctoral Researcher. Later, he was an Assistant Research Scientist at University of California, Los Angeles, as well as with the Goddard Earth Sciences and Technologies Center, University of Maryland Baltimore County, Baltimore, as an Associate Research scientist. His research interests are in remote sensing and radiative transfer. He has been actively conducting research in modeling of optical and radiative properties of clouds and aerosols, in particular, cirrus clouds and their applications to spaceborne and ground-based remote sensing.

Heli Wei received the M.S. degree in atmospheric physics from Anhui Institute of Optics and Fine Mechanics, Chinese Academy of Sciences, Hefei, in 1992.

He is currently a Senior Research Associate with the Department of Atmospheric Sciences, Texas A&M University, College Station. He has been conducting research in the infrared atmospheric radiative transfer, radiative properties of clouds, and remote sensing of cirrus clouds with high-resolution IR spectra.

Bryan A. Baum received the Ph.D. degree in atmospheric sciences from the Georgia Institute of Technology, Atlanta, in 1989.

He is currently a Senior Research Scientist with the Radiation and Aerosols Branch, NASA Langley Research Center (LaRC), Hampton, VA, but is stationed at the Cooperative Institute for Meteorological Satellite Studies (CIMSS), University of Wisconsin–Madison. His research activities have focused on satellite, aircraft, and surface-based remote sensing of multilayered cloud properties from multispectral imagery, regional and global cloud top property retrievals derived from satellite data, global fire and smoke detection, and the effect of clouds and aerosols on the earth's radiation budget.

Yongxiang Hu received the Ph.D. degree in atmospheric sciences from the University of Alaska, Fairbanks, in 1994.

He is currently a Senior Research Scientist at the Radiation and Aerosols Branch, NASA Langley Research Center, Hampton, VA. He was a Postdoctoral Researcher at the College of William and Mary, and a Research Professor at Hampton University before he joined NASA in 1999. His research interests include radiative transfer, passive and active atmospheric remote sensing, and satellite onboard data analysis.

Paolo Antonelli received the Ph.D. degree in atmospheric sciences from the University of Wisconsin, Madison (UW), in 2001.

He is currently a Research Scientist in the Space Science Engineering Center (SEEC), UW, and works for the Cooperative Institute for Meteorological Satellite Studies (CIMSS), UW. His research activities are focused on satellite, aircraft, and surface-based remote sensing of the atmosphere using high spectral resolution infrared observing systems. Specific areas of interest are data inversion (atmospheric temperature and water vapor retrievals, cloud property retrievals) and signal processing (principal component noise filtering).

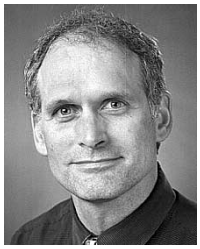

Steven A. Ackerman received the Ph.D. degree in atmospheric sciences from Colorado State University, Fort Collins, in 1987.

He joined the faculty of the Department of Atmospheric and Ocean Sciences, University of Wisconsin, Madison (UW), in 1992, where he is currently a Professor. He is also a Director of the Cooperative Institute for Meteorological Satellite Studies, UW, a position he has held since 1999. He is an Associate Member of MODIS Science Team, where he has primary responsibility for the MODIS cloud mask algorithm. His research experience includes remote sensing, radiative transfer, earth radiation budgets, cloud radiation parameterizations, climate change, and aerosol studies. In additional to his participation in MODIS Science Team, he is responsible for the cloud mask algorithm on the Global Imager (GLI), a sensor on Japan's ADEOS II spacecraft.